IOP Publishing Physica Scripta
Phys. Scr. 95 (2020) 065504 (11pp) https://doi.org/10.1088/1402-4896/ab7f4a

Quasiperiodic photonic crystals for filtering purpose by means of the n doped semiconductor material

Hussein A Elsayed

Physics Department, Faculty of Science, Beni-Suef University, Beni-Suef, Egypt

E-mail: drhussien85sc@gmail.com

Received 25 October 2019, revised 9 March 2020
Accepted for publication 12 March 2020
Published 2 April 2020

Abstract

We investigated the transmittance properties of the one dimensional quasiperiodic photonic crystals that contains an *n* doped semiconductor material. Our study is mainly based on the theoretical framework of the plasma model and the characteristic matrix method. Here, Fibonacci sequence represents the core axis in the design of our structure. Therefore, this design could be named as Fibonacci based structure. The numerical results are mainly based on the variation of the doping concentration. This parameter could be crucial in the tunability of the photonic band gaps. The effect of many parameters such as the thickness of the semiconductor material, the sequence number and the type of the sequence are demonstrated. The designed structure is prepared to act as a multichannel filter for THz applications.

Keywords: photonic crystals, photonic band gaps, quasiperiodic, fibonacci sequence, multichannel filter

(Some figures may appear in colour only in the online journal)

1. Introduction

Among the four past decades, the interaction of the electromagnetic radiations with the artificial periodic structures was significantly increased due to its role in many physical, optical and medical applications. These periodic structures are known later in the literature as photonic crystals (PCs). PCs are interested in the confining and guiding of the incident electromagnetic waves because of the appearance of the photonic band gaps (PBGs) and the photon localization [1–5]. The PBGs offer the ability of prohibiting the incident electromagnetic waves of specified frequencies from propagating through them [6–8]. The interference of Bragg scattering at the interfaces of the PCs constituent materials describes the physical interpretation of the appearance of these PBGs [9, 10]. Whilst, the periodic modulation of the refractive indices of PCs constituent materials could lead to such scattering [9, 10]. On the other side, the guiding of the incident electromagnetic waves or the photon localization is produced due to the broken periodicity of PCs by adding or removing a layer from the periodic structure. Here, the disordered PCs grants the opportunity of the presence of one or more of the discontinuous electromagnetic waves inside the PBG [4]. The previous characteristics of PCs could be crucial in the design and fabrications of many optical, physical and medical applications such as filters [11], optical reflectors [12], switches [13], gas sensing [14], integrated circuits [15], light harvesting for solar applications [16, 17] and biomedical sensors [18, 19]. Moreover, PCs are topping the scene in many promising application such as structural color applications [20], clinical analysis and food poisoning [21] and cancer diagnosis [22].

In recent time, quasicrystals received a considerable attention in the field of PCs owing to their inherent characteristics. Quasiperiodic PCs presents the intermediate state between the ordered and disordered PCs [23]. In addition, quasiperiodic PCs have the advantage over the traditional PCs on controlling the number and the width of the PBGs due to the appearance of more than one form of periodicity through these structures [23–27]. Whereas, quasiperiodic structures could be designed in many different sequences such as Fibonacci, Thue—Morse, period doubling and Rudin—Shapiro [28].

Moreover, quasicrystals are preferred in photon localization because of its weakness decay and rich self-similar structure [29].

In this paper, we theoretically study the transmittance characteristics of the one dimensional quasiperiodic PCs that containing an extrinsic semiconductor of *n* type (*n* InSb). Here, we aim to use the Fibonacci sequence to design our quasiperiodic PCs. The cornerstone of our study is basically depending on the effect of the doping concentration on the transmittance properties. Wherein, the doped semiconductor materials are widely used in the design of PCs because of their peculiar optical properties [30, 31]. Such materials could investigate the tunability of the PBGs at high values of the doping level [32].

Actually, the idea of using traditional and quasiperiodic PCs for filtering purposes is widely discussed [3, 33]. The results investigated in (3) discuss the ability of using traditional PCs for filtering applications in the visible light regions. In addition, Elsayed *et al* [33] demonstrated the transmittance properties of quasiperiodic PCs in the optical wavelengths using nanocomposite and plasma layers. However, the present work studies the same idea in a different wavelength regions. Our idea is mainly based on the role of quasiperiodic PCs in the tunability of the PBGs as investigated in ref. (3, 33). Thus, we intend to drive this advantage within the THz regions due to the huge number of applications through it. Whilst, this region represents the cornerstone of many medical, engineering and telecommunications applications [34, 35].

Therefore, the inclusion of quasiperiodic sequences in the one dimensional PCs through THz frequencies received a considerable attention. Many researchers devoted the attention towards the tunability of the PBGs within these frequencies using many different materials such as dielectrics, negative index materials, graphene and superconductors [36–39]. Moreover, Vyunishev *et al* demonstrated theoretically and experimentally the tunability of the PBGs in the visible light based on the one dimensional quasiperiodic PCs [40]. Such work investigated the formation of only two PBGs within the wavelengths of interest. In addition, the parameters of the constituent materials are not almost effecting on the tunability of the PBGs. Thus, we intend to design a structure that could provide the advantages over the previous work in controlling the width, number and the positions of the PBGs. Moreover, the need for special conditions of some materials particularly superconductors could increase the difficulty of the experimental verifications of these structures.

The theoretical model used to investigate the numerical results is prepared based on the fundamentals of the characteristic matrix method and the plasma model. The numerical results indicates the appearance of a multichannel filter within a broad band of the THz frequencies. Moreover, the doping concentration, the thickness of the semiconductor layer, the sequence number and the sequence type play an important role on the number and the positions of the bands of this filter.

This paper is organized according to the following pattern. In section 2, we investigate a brief description of the theoretical model. In section 3, we discuss the numerical results. Finally, section 4 recapitulates the conclusions of our paper.

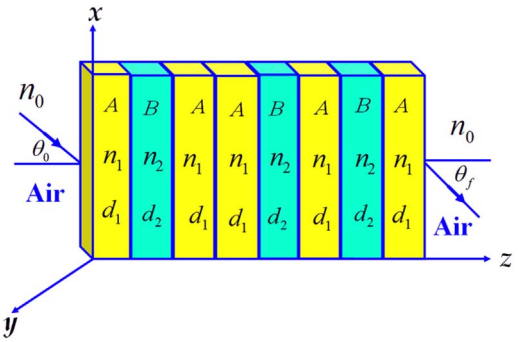

Figure 1. Schematic diagram of the designed one dimensional quasiperiodic PCs of F_5 in which the dielectric layer is labeled as A with thickness d_1 and refractive index n_1. The n InSb is set as layer B of thickness d_2 and refractive index n_2.

2. Theoretical model

In this section, we present a brief description to the characteristic matrix method and the plasma by which the numerical results are investigated. Such method is used to express the interaction between the incident electromagnetic waves and the macroscopic media [33]. The one dimensional quasiperiodic PCs is composed of a layers of the *n* doped semiconductor material (*n* InSb) that stacked with dielectric ones (SiO_2) in such manner according to the Fibonacci sequence. Here, the semiconductor layer is defined with the symbol (*S*) while the dielectric one is named as (*D*). Then, the whole structure is immersed within the air. Wherefore, the Fibonacci sequence used to build up our design can be obtained as, $F_{j+1} = F_j F_{j-1}$ for $j \geqslant 1$ with $F_0 = \{B\}$ and $F_1 = \{A\}$ thus $F_2 = F_1 F_0 = \{AB\}$, $F_3 = F_2 F_1 = \{ABA\}$ and so on [23].

Figure 1 describes the schematic diagram of the one dimensional quasiperiodic PCs based on Fibonacci type of F_5. This figure was drawn to clarify the nature of the interaction between our designed quasiperiodic PCs and the incident electromagnetic waves. Such type of interactions was explained using the characteristic matrix method [41–43].

In what follow, we present some of the basic details that are considered the core axis of the characteristic matrix method. Here, the *z* direction is set to be the direction of the propagating electromagnetic waves through our design. In other words, the electric and the magnetic field of the incident electromagnetic waves are propagating through the (*x*–*z*) plane.

For TE polarization in which the electric field is along *x* direction, the electric and magnetic fields through a given layer j of Fibonacci based structure can be described based on Maxwell's equations as,

$$\hat{E}_j(x,\ z) = E_j(z)\exp\left[i(k_x x - \omega t)\right]\hat{x}$$
$$\hat{H}_j(y,\ z) = H_j(z)\exp\left[i(k_x x - \omega t)\right]\hat{y} \qquad (1)$$

Where, E_j (z) and H_j (z) are the electric and magnetic field components through the layer j and can be written as,

$$E_j(z) = U_j \exp(-ik_j z) + V_j \exp(ik_j z)$$
$$H_j(z) = \frac{k_j}{k_0}[-U_j \exp(-ik_j z) + V_j \exp(ik_j\, z)]$$
$$k_j = k_0 n_j = (2\pi/\lambda) n_j \quad (2)$$

Where, U_j and V_j are the electric and magnetic field amplitudes in the layer j, respectively, k_j is the wave vector in layer j and n_j describes the refractive index of layer j. Equation (2) can be simplified using a matrix form as,

$$\begin{pmatrix} E_j(z) \\ H_j(z) \end{pmatrix} = \begin{pmatrix} \exp(-i\, k_j z) & \exp(i\, k_j z) \\ -n_j \exp(-i\, k_j z) & n_j \exp(i\, k_j z) \end{pmatrix} \begin{pmatrix} U_j \\ V_j \end{pmatrix} \quad (3)$$

Taking the inverse of equation (3), the field amplitudes in layer j could be calculated. Then, by applying the previous form, at the boundaries between two consecutive layers j and (j + 1), E_j (y) and H_j (y) take the form,

$$\begin{pmatrix} E_j(z) \\ H_j(z) \end{pmatrix} = \frac{1}{2} \begin{pmatrix} [\exp(-i\, k_j \xi_j) + \exp(i\, k_j \xi_j)] & \left[\dfrac{\exp(-i\, k_j \xi_j) - \exp(i\, k_j \xi_j)}{\delta_j}\right] \\ \delta_j [\exp(-i\, k_j \xi_j) - \exp(i\, k_j \xi_j)] & [\exp(-i\, k_j \xi_j) + \exp(i\, k_j \xi_j)] \end{pmatrix} \begin{pmatrix} E_{j+1}(z) \\ H_{j+1}(z) \end{pmatrix} \quad (4)$$

Using the expressions of sine and cosine functions, equation (4) can be written as,

$$\begin{pmatrix} E_j(z) \\ H_j(z) \end{pmatrix} = \begin{pmatrix} \cos(\, k_j \xi_j) & -i \sin(k_j \xi_j)/\delta_j \\ -i\delta_j \sin(k_j \xi_j) & \cos(\, k_j \xi_j) \end{pmatrix} \times \begin{pmatrix} E_{j+1}(z) \\ H_{j+1}(z) \end{pmatrix} = m_j \begin{pmatrix} E_{j+1}(z) \\ H_{j+1}(z) \end{pmatrix} \quad (5)$$

Where, $\xi_j = d_j \cos\theta_j$, $\delta_j = (\sqrt{\varepsilon_0/\mu_0})\, n_j \cos\theta_j$ for the case of TE polarization, θ_j defines the incident angle within layer j and m_j presents the characteristic matrix that relates E_j (z) and H_j (z) at the boundaries between two adjacent layers j and $j + 1$. Therefore, the whole interaction within Fibonacci based structure is described by:-

$$M = \begin{pmatrix} M_{11} & M_{12} \\ M_{21} & M_{22} \end{pmatrix} = \prod_{j=1}^{n} m_j \quad (6)$$

Wherefore, the transmittance coefficient is given as:-

$$t = \frac{2\delta_0}{(M_{11} + M_{12}\delta_0)\delta_0 + (M_{21} + M_{22}\delta_0)} \quad (7)$$

Then, the transmittance can be given as:-

$$T = |t^2| \quad (8)$$

For the case of TM polarization, we can use equations (5)–(8) but with $\delta_j = (\sqrt{\varepsilon_0/\mu_0})\, \cos\theta_j/n_j$

The other side of our theoretical model is specialized for the plasma model to investigate the permittivity of the n doped semiconductor material. This model describes the variation of the permittivity with the frequencies of the incident electromagnetic waves [30–32], as:-

$$\varepsilon(\omega) = \varepsilon_\infty \left(1 - \frac{\omega_{pe}^2}{\omega^2 - i\tau_e\omega} - \frac{\omega_{ph}^2}{\omega^2 - i\tau_h\omega} - \frac{\omega_T^2 - \omega_L^2}{\omega_T^2 - \omega^2 + i\gamma\omega}\right) \quad (9)$$

Where, ε_∞ is the high limit of the relative permittivity, ω is the frequency of the incident electromagnetic waves, $\omega_{pe(h)}$ is the electrons (holes) plasma frequency, $\tau_{e(h)}$ is the damping frequency due to electrons (holes), $\omega_{T(L)}$ is the transverse (longitudinal) optical phonon frequency and γ is the damping frequency due to phonons. The damping frequency due to electrons (holes) could be expressed as a function of electrons (holes) mobilities $\mu_{e\,(h)}$ as:-

$$\tau_{e(h)} = \frac{e}{m_{e(h)}\mu_{e(h)}} \quad (10)$$

Here, the carrier mobilities are strongly depending on the temperature by:-

$$\mu_e = 7.7 \times 10^4 \left(\frac{T}{300}\right)^{-1.66} \quad (11a)$$

$$\mu_h = 850 \left(\frac{T}{300}\right)^{-1.8} \quad (11b)$$

Then, the electrons (holes) plasma frequency can be obtained as a function of the carrier concentrations and the effective mass as:-

$$\omega_{pe(h)} = \sqrt{\frac{n_{e(h)} e^2}{m_{e(h)}\varepsilon_0\varepsilon_\infty}} \quad (12)$$

Where, $m_{e(h)}$ is the electrons (holes) effective mass, e is electronic charge, ε_0 is the permittivity of vacuum and $n_{e(h)}$ is the electrons (holes) concentration in the conduction (valence) band that could be described in terms of the doping impurity concentration as:-

$$n_{e(h)} = \sqrt{n_i^2 + \frac{N_d^2}{4}} \pm \frac{N_d}{2} \quad (13)$$

Where, n_i is the concentration of the intrinsic electrons and N_d is the concentration of the doping impurity. Here, the concentration of the intrinsic electrons is temperature dependent and could be written as:-

$$n_i = 5.76 \times 10^{20}\, T^{1.5} \exp(-0.13/k_B T) \quad (14)$$

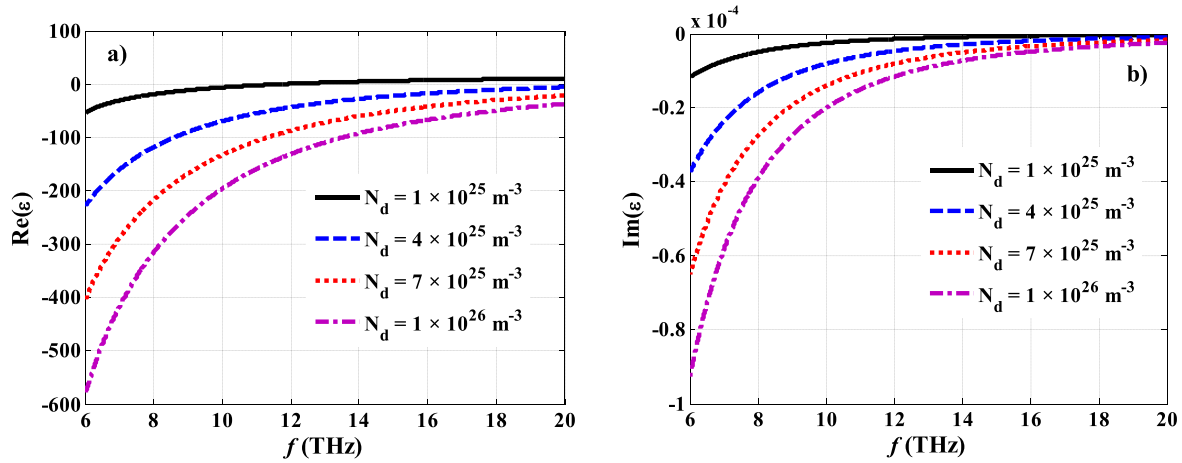

Figure 2. The response of the n InSb permittivity with the frequency of the incident electromagnetic waves at different values of the doping concentration for, (a) real part and (b) imaginary part.

3. Results ad discussions

Now, we present here the numerical results of our design reliance on the theoretical model described in the previous section. Here, we demonstrate the transmittance properties of the one dimensional quasiperiodic PCs through a broad band of the frequencies of the incident electromagnetic waves at normal incidence. This band is expanded from 6 THz to 20 THz and our results are investigated for the case of F_9. The cornerstone of our results is mainly based on the effect of the characteristics of the doped semiconductor material on the transmittance characteristics of Fibonacci based structure. Thus, we set the n doped semiconductor material to be (n InSb) of thickness equals 100 nm, $\varepsilon_\infty = 15.6$, $\omega_T = 35$ THz, $\omega_L = 37$ THz, $\gamma = 0.0539$ Hz, $m_h = 0.3827\ m_0$, $m_e = 0.014\ m_0$ and the value of the intrinsic electrons concentration is equivalent to 1.98×10^{22} m^{-3} at room temperature [31]. Then, the dielectric material is chosen to be SiO_2 of thickness $= 20\ \mu$m and refractive index is obtained based on the wavelength dependent Sellmeier equation as [44],

$$n^2 = 1.31552 + \frac{0.788404\ \lambda^2}{\lambda^2 - 0.0110199} + \frac{0.91316\ \lambda^2}{\lambda^2 - 100} \quad (15)$$

First, we demonstrate the effect of the doping impurity concentration on the permittivity of doped semiconductor material through the frequency of interest. Figure 2 indicates the variations of both the real and imaginary parts of n InSb permittivity. Figure 2(a) describes the response of the real values of the permittivity with the increase of the doping concentration. The figure indicates that the doping concentration has a significant effect on the real values of the permittivity especially at low values of the frequencies of interest. At $N_d = 1 \times 10^{25}$ m^{-3}, the values of the permittivity are varying from zero to 19.89 through a band of frequencies from 11.81 to 20 THz. For frequencies smaller than 11.81 THz, the response of the permittivity begins to take another pattern towards the negative values to reach 51 at 6 THz. As the value of the doping concentration increased to 4×10^{25} m^{-3}, the values of the permittivity are almost negative along all of the frequencies of the incident electromagnetic waves. For further increase of N_d to 7×10^{25} m^{-3} and 1×10^{26} m^{-3}, the real values of the permittivity take very large values in the negative side particularly at low frequencies as observed in figure 2(a). For the case of the imaginary part of the permittivity, its values are almost negative with the variation of the doping concentration as shown in figure 2(b). Moreover, its values increase with the increments of N_d values. However, these values are very small in comparable with the values of the real part of the permittivity. Wherefore, figure 2 demonstrates the role of the doping concentration on the values of the n InSb permittivity along the frequencies of interest. Such role leads the permittivity towards large negative values which could be of interest in prohibiting the propagation of the incident electromagnetic waves [32].

Then, figure 3 investigates the comparison between the transmittance characteristics of the one dimensional traditional PCs and those of the one dimensional quasiperiodic PCs. The one dimensional PCs is composed of a layer of n InSb staked together with a layer SiO_2 for 30 number of periods that is equivalent to 60 layers equally between SiO_2 and n InSb materials. On the other side, the one dimensional quasiperiodic PCs is designed from the same materials for the case of F_9 which can be designed using 55 layers of SiO_2 and n InSb materials but with not equal number. Moreover, the doping concentration value of n InSb is the same for the two structures and its equivalent to 4×10^{25} m^{-3}. Figure 3(a) shows the transmittance properties of the perfect PCs. As shown in the figure, there are two PBGs are formed along the frequencies region of the incident electromagnetic waves. The first one has a width of 1.3 THz because it extends from 10.21 to 11.51 THz. The second PBG appears between 15.33 and 16.03 THz with width 0.7 THz. For the case of the quasiperiodic PCs, the number of the PBGs formed within the frequency of interest is six PBGs with varied widths as shown in figure 3(b). Here, the number of the PBGs in the case quasiperiodic is greater than the case of the perfect PCs. This pattern clarifies the role of the quasiperiodic in controlling the number and the width of the PBGs due to the different forms of periodicity through the same structure. Therefore, the large number of the PBGs gives the advantage for the quasiperiodic PCs over the perfect PCs and could grant more facilities in the design of the proposed multichannel filter. In particular, the number of layers used to design the quasiperiodic PCs of F_9 is smaller than

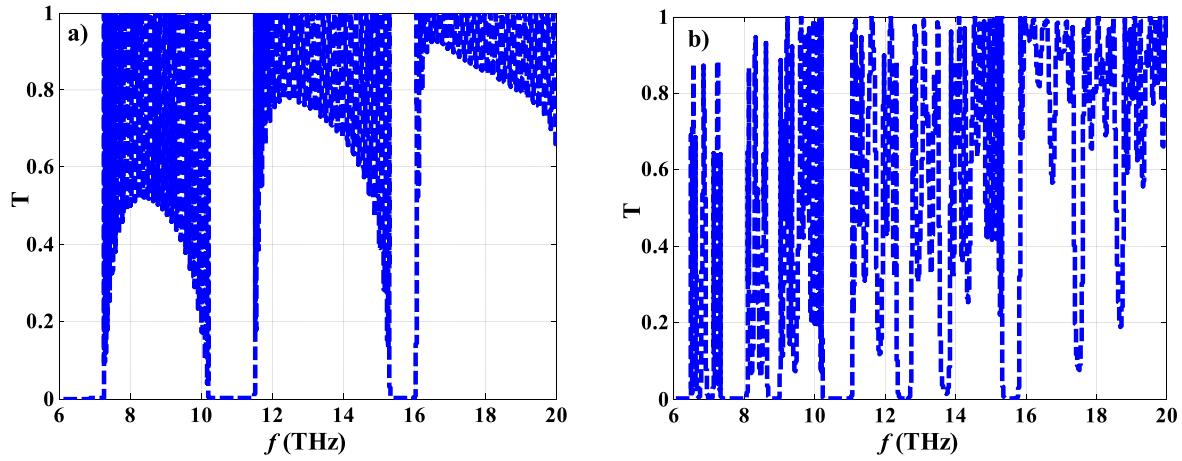

Figure 3. The transmittance properties versus the frequency of the incident electromagnetic waves at $N_d = 4 \times 10^{25}$ m^{-3} for, (a) perfect one dimensional PCs and (b) one dimensional quasiperiodic PCs.

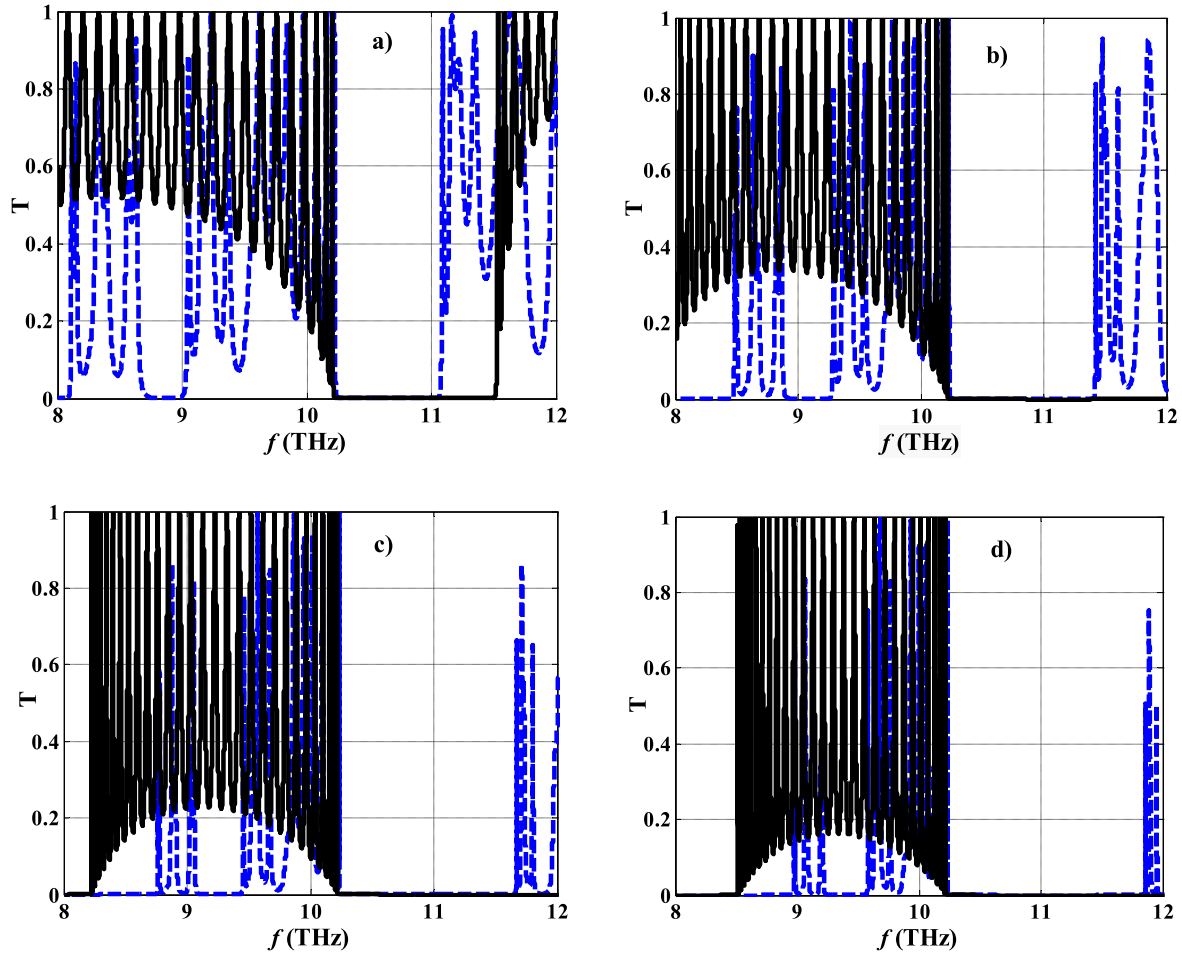

Figure 4. A detailed description of the transmittance characteristics of both perfect one dimensional PCs of periodicity = 30 (solid black line) and one dimensional quasiperiodic PCs of F_9 at different values of the doping concentration, (a) $N_d = 4 \times 10^{25}$ m^{-3}, (b) $N_d = 6 \times 10^{25}$ m^{-3}, (c) $N_d = 8 \times 10^{25}$ m^{-3} and (d) $N_d = 1 \times 10^{26}$ m^{-3}.

that used to design the traditional PCs by 5 layers. Furthermore, all of these gaps appear at frequencies smaller than 16 THz because the permittivity of the *n* InSb material begins to take very large negative values at frequencies smaller than this frequency as investigated in figure 2. This response leads to the formation of these PBGs because of the high refractive index contrast between SiO_2 and *n* InSb within this frequencies region.

Then, we clarified in details the novelty of the quasiperiodic PCs over the perfect PCs on the tunability of the PBG as shown in figure 4. Here, our comparison is summarized through the

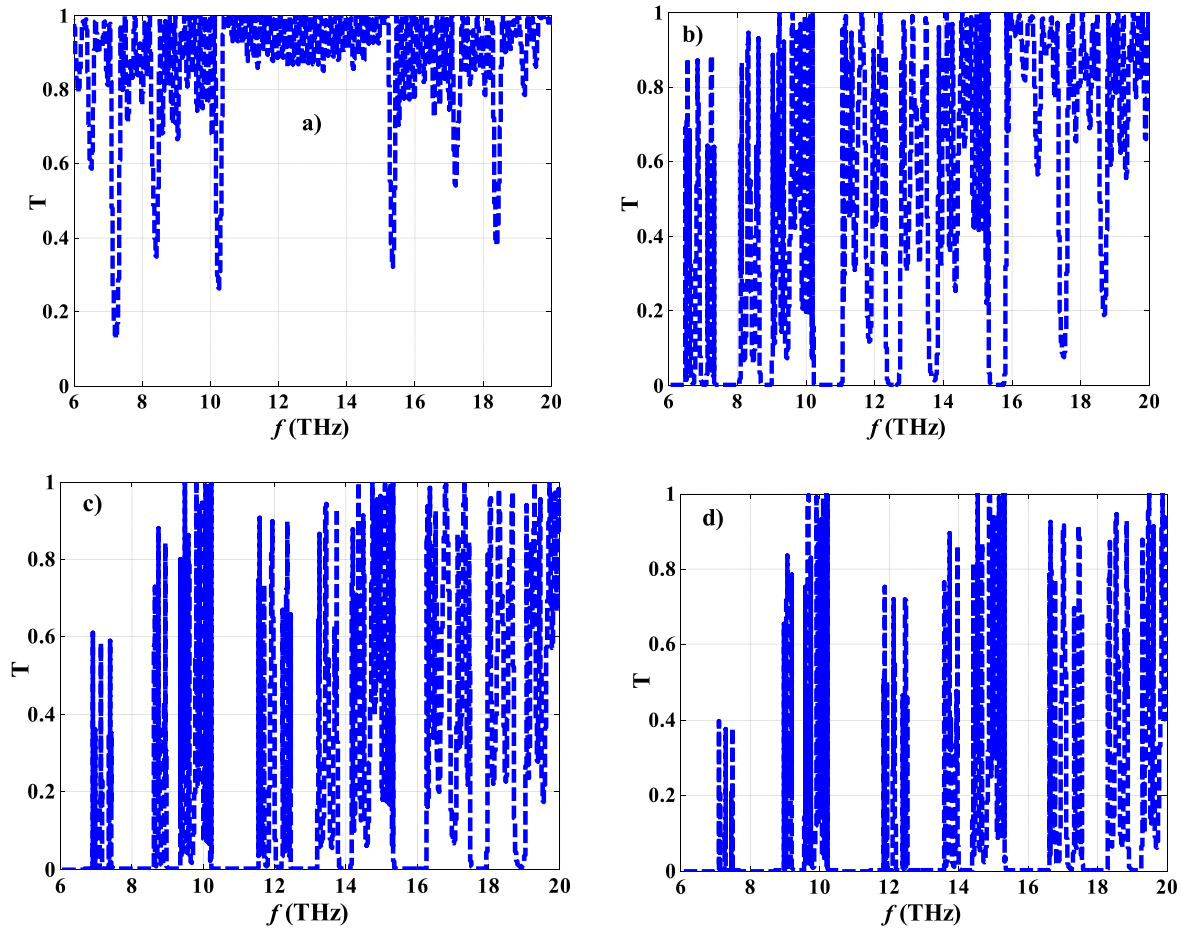

Figure 5. The dependence of the transmittance properties of the one dimensional quasiperiodic PCs on the doping impurity concentration of n InSb material, (a) $N_d = 1 \times 10^{25}$ m^{-3}, (b) $N_d = 4 \times 10^{25}$ m^{-3}, (c) $N_d = 7 \times 10^{25}$ m^{-3} and (d) $N_d = 1 \times 10^{26}$ m^{-3}.

frequency regions from 8 to 12 THz. Moreover, the number of periods for the perfect PCs is set to be 30 and the sequence number of the quasiperiodic PCs is F_9. At $N_d = 4 \times 10^{25}$ m^{-3}, only one PBG can be formed within the perfect PCs of frequency limits of 10.21 and 11.52 THz as shown in figure 4(a). On the other side, the quasiperiodic PCs show the appearance of two PBGs within the frequencies of interest of frequency limits (8.68–9.01 THz) and (10.21–11.07 THz). As the doping concentration value increased to $N_d = 6 \times 10^{25}$ m^{-3}, $N_d = 8 \times 10^{25}$ m^{-3} and $N_d = 1 \times 10^{26}$ m^{-3}, the central PBG of the perfect PCs is shifted towards the high frequencies with the increasing in its width as shown in figures 4(b)–(d), respectively. In addition, a new PBG begins to appear at frequencies smaller than 8.23 THz. This new PBG is shifted towards the high frequencies with the increase of the doping concentration. Moreover, the transmission dips (oscillations) of frequencies below the lower edge of the central PBG begins to shrink with the increase of the doping concentration as shown in figures 4(c) and (d), respectively. Furthermore, the amplitudes of these oscillations are providing a significant decrements. This response could be due to the change in the permittivity of InSb layer with the variation of its doping concentration. For the case of quasiperiodic PCs, the number and the widths begins to increase with the doping concentration. Such response could be of interest in the design of our multichannel filter particularly through small frequency regions.

Now, we demonstrate the effect of the doping concentration on the transmittance characteristics of our one dimensional quasiperiodic PCs as shown in figure (5). The figure clarifies the significant effect of the doping concentration on the number and the width of the formed PBGs. This effect appears as a power result of the variation of *n* InSb permittivity with the doping concentration as investigated in figure 2. At $N_d = 1 \times 10^{25}$ m^{-3}, no PBGs are formed as shown in figure 5(a). Here, the absence of the PBGs is due to the small value of *n* InSb permittivity at this value of the doping concentration especially at high frequencies as investigated in figure 2. This response weakens the possibility of the PBGs formation because of the small contrast between *n* InSb and SiO_2 materials. As the value of N_d increased to 4×10^{25} m^{-3} and 7×10^{25} m^{-3}, the PBGs begin to appear along the frequencies region of the incident electromagnetic waves as shown in figures 5(b) and (c), respectively. For $N_d = 1 \times 10^{26}$ m^{-3}, the number of the PBGs increased beside the presence of the resonant peaks at low frequencies as shown in figure 5(d). Accordingly, the doping impurity concentration could be of interest in controlling the width and the number of the PBGs that formed through the frequencies of the incident electromagnetic waves.

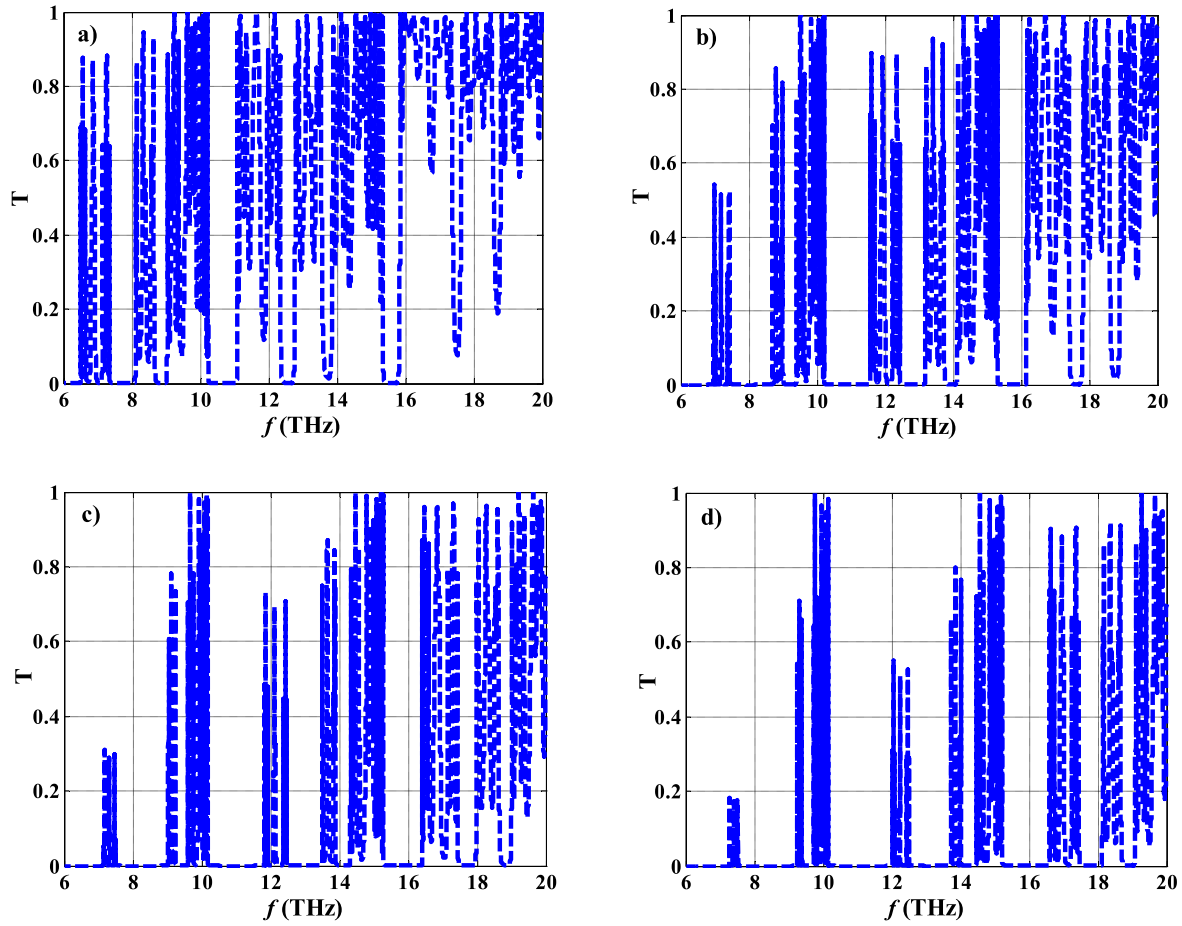

Figure 6. The transmittance properties dependence on the thickness of n InSb at constant value of the doping concentration ($N_d = 4 \times 10^{25}$ m^{-3}) for, (a) d = 100 nm, (b) d = 200 nm, (c) d = 300 nm and (d) d = 400 nm.

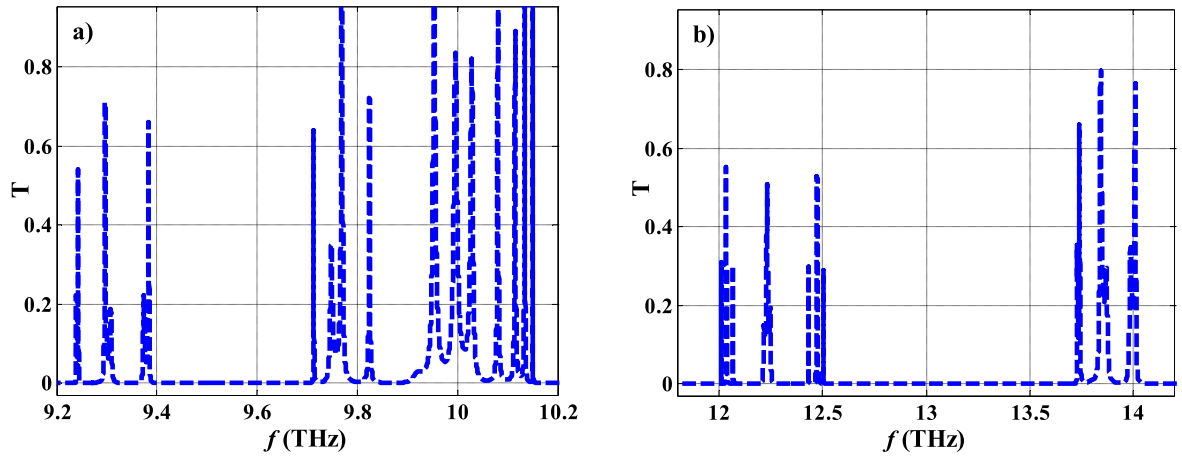

Figure 7. The response of the resonant peaks at constant values of the doping concentration and constant thickness of n InSb material (d = 400 nm) through two different frequencies regions.

In what follows, we present the effect of some parameters on the transmittance characteristics of Fibonacci based structure at constant value of the doping concentration. Wherein, N_d is set to equal 4×10^{25} m^{-3}. Figure 6 describes the transmittance properties at different values of the thickness of *n* InSb material. As the thickness increased from 100 to 200, 300 and 400 nm, the number and the width of the PBGs are significantly affected particularly in the high frequencies region as shown in figures 6(b)–(d), respectively. Therefore, the thickness of the n InSb material could investigate the role of the doping impurity concentration in controlling the number and the width of the PBGs. In other words, the increase of thickness of the doped semiconductor offers the possibility to overcome the high values of the doping concentration.

Furthermore, the resonant peaks appear frequently with varying transmittance values as shown in figure 7. Figure 7

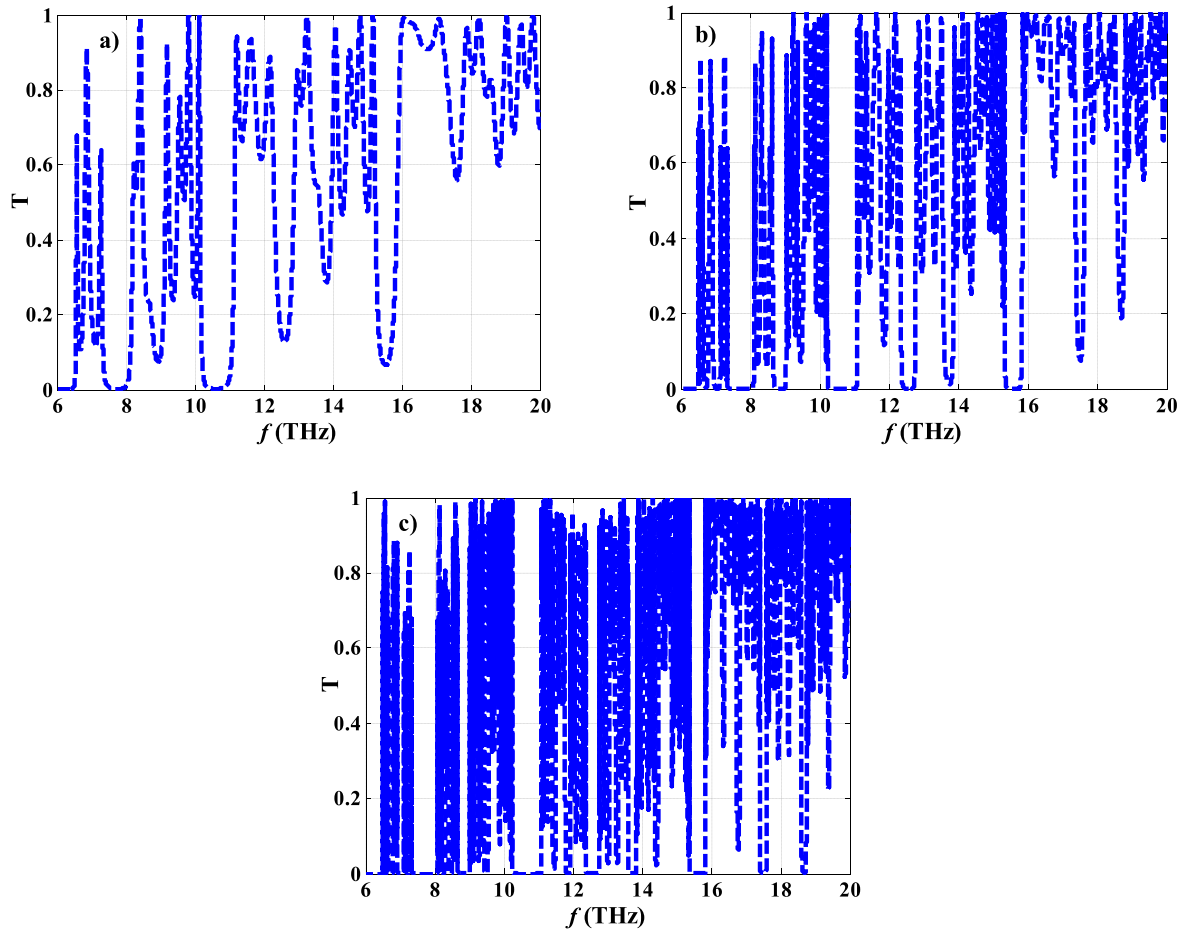

Figure 8. The variation of transmittance with the sequence number of our design for, (a) F_7, (b) F_9 and (c) F_{11}.

indicates the appearance of resonant peaks when the thickness of n InSb material equals 400 nm at two specified frequencies regions. In the case of the perfect PCs, the appearance of these resonant peaks needs for the breaking of the structure periodicity by adding a new layer with different values of refractive index or thickness or both of them. However, figure 7 clarifies that the appearance of this peaks is not subject with the breaking of the structure periodicity [4, 14, 18, 19]. In other words, the quasiperiodic PCs provide the presence of the resonant peaks that could be of interest in many applications especially in optical and medical sensing. Moreover, the number and positions of the resonant peaks within the perfect PCs require some conditions to obtain them unlike the quasiperiodic PCs [4]. This response could be due to the nature of the quasiperiodic structures as an intermediate state between the ordered and disordered structures. Thus, this response could offer another advantage in the design of our multichannel filter.

Then, we discuss the effect of the number of sequence on the transmittance response of our design as shown in figure 8. Figure 8(a) investigates the transmittance properties for the case of F_7. The figure shows the appearance of only two PBGs in the low frequencies region. As the sequence number increased to F_9 and F_{11}, the number of the PBGs begins to increase especially through the high frequencies region as shown in figures 8(b) and (c), respectively. Moreover, the edges of the PBGs begin to be sharper as comparable with the case of F_7. Here, the increment of the sequence number leads to due to more forms of periodicity that could be effective in the tunability of the PBGs.

Now, we demonstrate the effect of the different sequences as shown in figure 9. The figure describes the transmittance in the cases of Fibonacci of sequence number 9, Thue Morse of sequence number 6 and the period doubling of sequence number 6. The sequence number of Thue Morse could be configured as $T_{j+1} = T_j\, inv\,(T_j)$ for $j \geqslant 1$ with $T_0 = \{A\}$ and $inv\,(T_0) = \{B\}$ and $inv\,(T_{j+1}) = inv\,(T_j)\,T_j$ [44, 45]. Whilst, the double period sequence is obtained using, $P_{j+1} = P_j\, inv\,(P_j)$ for $j \geqslant 1$ with $P_0 = \{A\}$ and $inv\,(P_0) = \{B\}$ and $inv\,(P_{j+1}) = P_j\, P_j$ [45, 46]. In the case of Thue Morse, the transmittance takes a different manner in comparable with the case of Fibonacci as shown in figure 9(b). Here, the edges of the PBGs become sharper and their widths are larger. Furthermore, we observe the appearance of the resonant peaks through these PBGs. For the period doubling case, it almost takes a similar pattern as Thue Morse as shown in figure 9(c). However, the widths of the PBGs and the transmittance values of the resonant peaks are smaller than the case of Thue Morse sequence.

NHere, we demonstrate the effect of temperature on the transmittance characteristics of Fibonacci based structure. Figure 10 discusses the transmittance response at different

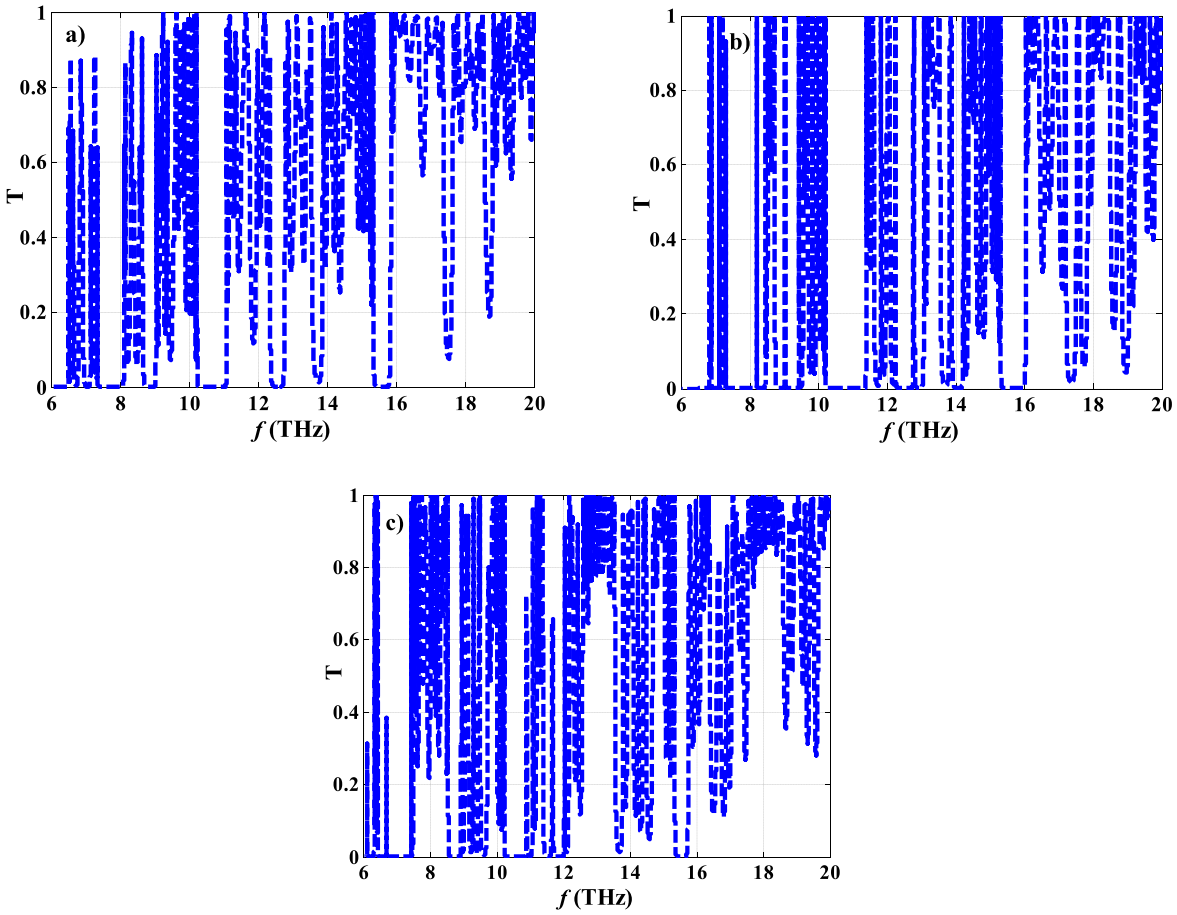

Figure 9. The dependence of the transmittance on the sequence type for, (a) Fibonacci sequence, (b) Thue Morse sequence and (c) The period doubling sequence.

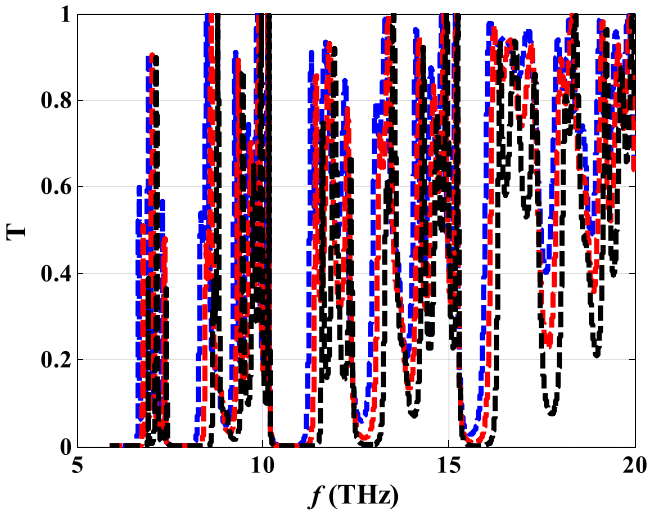

Figure 10. The dependence of the transmittance on the temperature of Fibonacci based structure at, 300 K (dashed blue), 400 K (dashed red) and 500 K (dashed black) for F_7 sequence.

values of the temperature. We set the sequence number F_7 and the value of $N_d = 4 \times 10^{25}$ m^{-3}. The figure shows a distinct effect to the temperature on the transmittance characteristics of Fibonacci based structure. This effect appears in the form of the decrements of the transmissio values with temperature and the expanding of the PBGs towards the high frequencies as well. This response of the transmittance spectrum can be simply understood from the strong dependence of the *n* InSb layer on the temperature. On the other side, the refractive index of SiO_2 is slightly effected with temperature in comparison with *n* InSb layer because of the small thermo-optic coefficient of SiO_2. Thus, the change in the permittivity of n InSb layer could change the width of the PBGs. As the temperature increased from 300 K (blue) to 400 K (red) and 500 K (black), the width of the PBGs begins to increase due to the shift of the upper edges towards the high frequencies. In comparing with equation (14) through the theoretical analysis, the concentration of the intrinsic electrons increase with the temperature. Such effect leads to the increase of the electrons concentrations and their plasma frequency as well. Thus, a significant changes in the permittivity of InSb layer is expected. Wherefore, the transmission characteristics of the PBGs are affected as shown in the figure. Thus, the sensitivity of the proposed structure could be affected with the change of the temperature. Here, Fibonacci based structure provides a sensitivity of 0.0021 THz/K. Therefore, this property could make our design of valuable interest in the temperature sensing applications.

4. Conclusion

In summary, we investigated theoretically the transmittance properties of the one dimensional quasiperiodic PCs in THz regime. The proposed structure is composed of a dielectric material (SiO_2) and an *n* doped semiconductor material (*n* In Sb) that designed based on Fibonacci sequence. Therefore, the numerical results are obtained based on the plasma model and the characteristic matrix model. The cornerstone of our study is mainly depending on the doping impurity concentration of the semiconductor material. Wherefore, the permittivity of *n* InSb is strongly affected with the doping concentration variations. The numerical results show that the quasiperiodic PCs is more promising in the tunability of the PBGs than the perfect PCs. Moreover, the doping impurity concentration could be of interest in controlling the width and the number of the PBGs that formed through the frequencies of interest. In addition, the increase of thickness of the doped semiconductor has the same effect on the properties of our design as the increase of the doping concentration. Thus, it could offer the possibility to overcome the high values of the doping concentration. Furthermore, the number and the type of sequence offer the advantage of controlling the width, position and number of the PBGs beside the appearance of the resonant peaks. Finally, Fibonacci based structure could be of interesting to act as a multichannel filter for THz applications ranging from 6 to 16 THz.

ORCID iDs

Hussein A Elsayed https://orcid.org/0000-0001-7819-9476

References

[1] Yablonovitch E 1987 Inhibited spontaneous emission in solid-state physics and electronics *Phys. Rev. Lett.* **58** 2059–62
[2] John S 1987 Strong localization of photons in certain disordered dielectric superlattices *Phys. Rev. Lett.* **58** 2486
[3] Elsayed H A 2018 A multi-channel optical filter by means of one dimensional n doped semiconductor dielectric photonic crystals *Mater. Chem. Phy.* **216** 191–6
[4] Aly A H and Elsayed H A 2012 Defect mode properties in a one-dimensional photonic crystal *Phys. B* **407** 120–5
[5] Elsayed H A 2019 Photonic band gaps properties of two-dimensional ternary superconductor photonic crystals *Surf. Rev. Lett.* **26** 1850152
[6] Barvestani J, Rezaei E and Vala A S 2013 Tunability of waveguide modes in two-dimensional photonic crystals based on superconducting materials *Opt. Commun.* **297** 74–8
[7] Elsayed H A, El-Naggar S A and Aly A H 2014 Thermal properties and two-dimensional photonic band gaps *J. Modern Opti.* **61** 385–9
[8] Aly A H, Sabra W and Elsayed H A 2017 Cutoff frequency in metamaterials photonic crystals within Terahertz frequencies *Int. J. Mod. Phys. B* **31** 1750123
[9] Aly A H, Elsayed H A and Hamdy H S 2010 The optical transmission characteristics in metallic photonic crystals *Mater. Chem. Phy.* **124** 856–60
[10] Elsayed H A 2018 Transmittance properties of one dimensional ternary nanocomposite photonic crystals *Mater. Res. Express* **5** 036209
[11] Kong H and Lee H-Y 2019 Thermal darkening of one-dimensional photonic crystal containing tellurium suboxide *Opt. Mater.* **88** 167–75
[12] Hadfield R H 2009 Single-photon detectors for optical quantum information applications *Nature Photon.* **3** 696–705
[13] Elsayed H A and Aly A H 2018 Terahertz frequency superconductor-nanocomposite photonic band gap *Int. J. Mod. Phys. B* **32** 1850056
[14] Chen Y-H, Shi W-H, Feng L, Xu X-Y and Shang-Guan M-Y 2019 Study on simultaneous sensing of gas concentration and temperature in one-dimensional photonic crystal *Superlatt. Microstr.* **131** 53–8
[15] Razi S and Ghasemi F 2019 Tunable graphene based one dimensional photonic crystal with applications in terahertz optical integrated circuits *Phys. B* **566** 77–85
[16] Mokkapati S and Catchpole K R 2012 Nanophotonic light trapping in solar cells *J. Appl. Phys.* **112** 101101
[17] Wu Y, Lu J, Li M, Yuan J, Wu P, Chang X, Liu C and Wang X 2019 Bismuth silicate photocatalysts with enhanced light harvesting efficiency by photonic crystal *J. Alloys Compd.* **810** 151839
[18] Abd El-Aziz O A, Elsayed H A and Sayed M I 2019 One-dimensional defective photonic crystals for the sensing and detection of protein *Appl. Opt.* **58** 8309–15
[19] Elsayed H A and Mehaney A 2019 A new method for glucose detection using the one dimensional defective photonic crystals *Mater. Res. Express* **6** 036201
[20] Dalmis R, Keskin O Y, Funda Ak Azem N and Birlik I 2019 A new one-dimensional photonic crystal combination of TiO_2/CuO for structural color applications *Ceram. Internat.* **45** 21333–40
[21] Qiu X, Chen W, Luo Y, Wang Y, Wang Y and Guo H 2020 Highly sensitive α-amanitin sensor based on molecularly imprinted photonic crystals *Anal. Chim. Acta* **1093** 142–9
[22] Li Q, Zhou S, Zhang T, Zheng B and Tang H 2020 Bioinspired sensor chip for detection of miRNA-21 based on photonic crystals assisted cyclic enzymatic amplification method *Biosen. Bioelectr.* **150** 111866
[23] Zhang H F, Zhen J P and He W P 2013 Omnidirectional photonic band gaps enhanced by Fibonacci quasiperiodic one-dimensional ternary plasma photonic crystals *Optik* **124** 4182 - 4187
[24] Silva E F, Costa C H, Vasconcelos M S and Anselmo D H A L 2019 Transmission spectra in graphene-based octonacci one-dimensional photonic quasicrystals *Opt. Mater.* **89** 623–9
[25] Trabelsi Y, Alia N B, Elhawil A, Krishnamurthy R, Kanzari M, Amiri I S and Yupapin P 2019 Design of structural gigahertz multichanneled filter by using generalized Fibonacci superconducting photonic quasicrystals *Results in Physics* **13** 102343
[26] Bellingeri M, Chiasera A, Kriegel I and Scotognella F 2017 Optical properties of periodic, quasi-periodic, and disordered one-dimensional photonic structures *Opt. Mater.* **72** 403–21
[27] Aly A H, Malek C and Elsayed H A 2018 Transmittance properties of a quasi-periodic one-dimensional photonic crystals that incorporate nanocomposite material *Int. J. Mod. Phys. B* **32** 1850220
[28] Steurer W and Widmer D S 2007 Photonic and phononic quasicrystals *J. Phys. D: Appl. Phys.* **40** R229
[29] Fujiwara T, Kohmoto M and Tokihiro T 1989 Multifractal wave functions on a Fibonacci lattice *Phys. Rev. B* **40** 7413

[30] Halevi P and Mendieta F R 2000 Tunable photonic crystals with semiconducting constituents *Phys. Rev. Lett.* **85** 1875
[31] Sanchez A S and Halevi P 2003 Simulation of tuning of one-dimensional photonic crystals in the presence of free electrons and holes *J. Appl. Phys.* **94** 797–9
[32] Elsayed H A, El-Naggar S A and Aly A H 2015 Two dimensional tunable photonic crystals and n doped semiconductor materials *Mater. Chem. Phys.* **160** 221–6
[33] Elsayed H A and Abadla M M 2020 'Transmission investigation of one-dimensional Fibonacci-based quasi-periodic photonic crystals including nanocomposite material and plasma *Phys. Scr.* **95** 035504
[34] Pickwell E and Wallace V P 2006 Biomedical applications of terahertz technology *J. Phys. D: Appl. Phys.* **39** R301–10
[35] Pawar A Y, Sonawane D D, Erande K B and Derle D V 2013 Terahertz technology and its applications *Drug Invention Today* **5** 157–63
[36] Araújo C A A, Vasconcelos M S, Mauriz P W and Albuquerque E L 2012 Omnidirectional band gaps in quasiperiodic photonic crystals in the THz region *Opt. Mater.* **35** 18–24
[37] Zhou D, Wang X, Zhu H and Shen F 2018 Graphene-based tunable multichannel filter with arithmetic sequence quasiperiodic structure *Optik* **174** 282–8
[38] Zhang Y, Wu Z, Cao Y and Zhang H 2015 Optical properties of one-dimensional Fibonacci quasi-periodic graphene photonic crystal *Opt. Commun.* **338** 168–73
[39] Segovia-Chaves F and Vinck-Posada H 2019 Transmittance spectrum of a superconductor-semiconductor quasiperiodic one-dimensional photonic crystal *Phys. C* **563** 10–5
[40] Vyunishev A M, Pankin P S, Svyakhovskiy S E, Timofeev I V and Vetrov S Y 2017 'Quasiperiodic one-dimensional photonic crystals with adjustable multiple photonic bandgaps *Opt. Lett.* **42** 3602–5
[41] Born M and Wolf E 1999 *Principles of Optics* (London: Cambridge)
[42] Li-gang W, Nian-hua L, Qiang L and Shi-yao Z 2004 'Propagation of coherent and partially coherent pulses through one-dimensional photonic crystals *Phys. Rev. E* **70** 016601
[43] Orfanidis S J 2008 *Electromagnetic Waves and Antennas* (Rutger University)
[44] Liu Q, Li S, Chen H, Li J and Fan Z 2015 High-sensitivity plasmonic temperature sensor based on photonic crystal fiber coated with nanoscale gold film *Appl. Phys. Expr.* **8** 046701
[45] Singh B K and Pandey P C 2014 Influence of graded index materials on the photonic localization in one-dimensional quasiperiodic (Thue—Mosre and Double—Periodic) photonic crystals *Opt. Communications* **333** 84–91
[46] Albuquerque E L and Cottam M G 2003 Theory of elementary excitations in quasiperiodic structures *Phy. Reports* **376** 225–337